

A Comparative Study Of Orthogonal Moments for Micro-Doppler Classification

Sabrina Machhour ^{*†}, Eric Grivel ^{*}, Pierrick Legrand [†], Vincent Corretja [‡] and Clement Magnant [‡]

^{*}Bordeaux University - INP Bordeaux ENSEIRB-MATMECA - IMS - UMR CNRS 5218, Talence, FRANCE

[†]Bordeaux University - IMB - INRIA, Talence, FRANCE

[‡] THALES DMS France, Merignac, FRANCE

Abstract—Micro-Doppler induced by mechanical vibrating or rotating structures in a radar target is possibly useful for its detection, classification and recognition. In a previous work, pseudo-Zernike moments (PZMs) were used as micro-Doppler features for classification. Despite of their promising classification rates, the choice of PZMs is debatable because other types of moments exist. In this paper, our purpose is to compare various kinds of micro-Doppler features such as Zernike moments, PZMs, orthogonal Mellin-Fourier moments, Legendre moments and Krawtchouk moments in order to evaluate which moments are the most relevant in terms of reconstruction ability, computational cost and micro-Doppler classification rate. Advantages and drawbacks of each family of moments are also given. Through the simulations we carried out, when the signal is disturbed by an additive white noise and the signal-to-noise ratio is low, the use of Krawtchouk moments as micro-Doppler features turns out to be the best compromise.

Index Terms—Radar, Micro-Doppler, Features, Moments, Classification.

I. INTRODUCTION

In radar processing, backscattered signals can include micro-Doppler information due to the mechanical vibrations and/or the rotations of some structures of the target [23]. In some cases, this phenomenon is considered as a disturbance that must be removed [24]. In other situations, this signature can be useful for the detection of the target, its recognition and its classification [9]. Some approaches [8], [21], [5] have been proposed based on time-frequency analysis to extract the micro-Doppler component from the received signal. In [4], the authors consider the so-called cadence velocity diagram (CVD), which is an image deduced from the spectrogram of the micro-Doppler signal. Then, as this is usually done in the field of vision or pattern recognition, they suggest using moments, which correspond to a weighted sum of the image pixels' intensities, to describe the CVD. These latter are used for classification. This method shows great promises for its reconstruction and classification ability, but only the pseudo-Zernike moments (PZMs) have been considered. This choice is debatable because various types of moments exist. They can be sorted by taking into account the orthogonality property:

- 1) The non-orthogonal moments include the general moments of order $n + m$. They consist of weighting the image intensity function $f(x, y)$ by a polynomial function $V_{n,m}(x, y)$ and summing over all the values of x and y . The most basic choice is the power basis where $V_{n,m}(x, y) = x^n y^m$ that leads to the so-called geometric

moments. The image centroid can be deduced from some of them. Another popular choice for the polynomial basis is $V_{n,m}(x, y) = (x + jy)^n (x - jy)^m$ which leads to the complex moments. Nevertheless, despite of their low computational cost, they may be rotational variant and highly sensitive to noise. In addition, due to the redundancy induced by their non-orthogonal property, reconstruction is difficult.

- 2) The so-called orthogonal moments can be split into two families: the continuous and the discrete ones. In addition, some of them are orthogonal on a unit disk whereas others are orthogonal on a rectangle. The Jacobi-Fourier moments (JFMs) are based on an image mapped into a unit disk. Zernike moments (ZMs), its variant known as PZMs and the orthogonal Fourier-Mellin moments (OFMMs) are special cases of JFMs since the radial polynomials of the ZMs, the PZMs and the OFMMs belong to the Jacobi polynomials [13]. The Gegenbauer polynomials, also known as ultra-spherical polynomials of order λ , are orthogonal over the square $[-1, 1] \times [-1, 1]$. When $\lambda = 0.5$, they correspond to Legendre polynomials. These latter are used to define the Legendre moments (LMs). Both Gegenbauer and Jacobi-Fourier moments form "continuous" families as their calculations are based on the computations of double integrations. As an alternative, discrete orthogonal basis such as Dual Hahn moments, Racah moments and Krawtchouk moments (KMs) can be used.

In this paper, micro-Doppler signals are analyzed and classified by following the same processing chain as the one proposed in [4]. Our purpose is to compare representatives of each family of orthogonal moments, namely ZMs, PZMs, OFMMs, LMs and KMs, in order to analyze which method is the most relevant in terms of reconstruction and classification ability as well as computational cost, when the signal is disturbed in the time-domain by an additive white noise. The rest of this paper is structured as follows: Section II recalls the main steps of the approach initially proposed in [4]. Each type of moment is presented. In section III, simulation results and comments are provided. Conclusions are then given.

In the following, $*$ is the conjugate, $n!$ is the factorial of n , $\Gamma(\cdot)$ is the Gamma function, $(a)_k = \frac{\Gamma(a+k)}{\Gamma(a)}$ is the Pochhammer symbol, $\text{sinc}(\cdot)$ denotes the cardinal sine function and $\delta(n, m)$ is the Kronecker delta function.

II. MAIN STEPS OF THE PROCESSING CHAIN

The processing chain, initially proposed by Clemente in [4], operates with the following steps:

A. Step 1: time-frequency (TF) representation

The micro-Doppler signal is first pre-processed to be zero-mean and unit-variance. Then, instead of analyzing a large amount of samples in the time-domain, a time-frequency analysis is considered to point out the variations of the micro-Doppler signal. Several methods can be used from the spectrograms, based on FFT or other spectral analysis methods (Music or Capon), to the Cohen classes.

B. Step 2: from TF representation to CVD

The CVD provides a measure of how often values of the Doppler frequency are repeated over time. It is obtained by computing the spectrogram of the time-frequency representation along each frequency bin. It is an image, with cadence in abscissa x and frequency in ordinate y .

C. Step 3: feature extraction based on moments

The CVD is projected onto a set of predefined images leading to the moments. In [4], PZMs were considered. Before presenting the three families of moments, let us first define the Jacobi polynomials. They will be useful in the following.

$$P_n(\alpha, \beta, x) = \frac{\Gamma(\alpha + n + 1)}{\Gamma(\alpha + \beta + n + 1)!} \times \sum_{k=0}^n \frac{\Gamma(n + k + \alpha + \beta + 1)!}{k!(n - k)!\Gamma(\alpha + k + 1)!} \left(\frac{x - 1}{2}\right)^k \quad (1)$$

The polynomials $P_n(\alpha, \beta, x)$ and $P_m(\alpha, \beta, x)$ are orthogonal with respect to the weights $(1 - x)^\alpha(1 + x)^\beta$ with $x \in [-1, 1]$.

1) JFMs including ZMs, PZMs and OFMMs:

JFMs have been widely used as feature extractors of an image in several applications from face recognition [6] to image denoising [15]. Denoted as $M_{n,m}^{JFM}$, JFMs of non-negative integer order n and repetition m , which is an integer positive or negative, are computed on the image $f(r, \theta)$ on the unit disk with polar coordinates (r, θ) , with $r = \sqrt{x^2 + y^2}$ and $\theta = \arctan(\frac{y}{x})$. They correspond to the projection of the CVD onto the kernel functions, $J_{n,m}(p, q, r, \theta)$ with p and q real parameters:

$$M_{n,m}^{JFM} = \int_0^{2\pi} \int_0^1 f(r, \theta) \mathbf{J}_{n,m}^*(p, q, r, \theta) r dr d\theta \quad (2)$$

Using [1], the kernel function $\mathbf{J}_{n,m}(p, q, r, \theta)$ is expressed as the product of the radial factor $b_n(p, q, r)J_n(p, q, r)$ and the angular (Fourier) factor $\omega_m(\theta) = \frac{1}{\sqrt{2\pi}}e^{jm\theta}$:

$$\mathbf{J}_{n,m}(p, q, r, \theta) = b_n(p, q, r)J_n(p, q, r)\omega_m(\theta) \quad (3)$$

where $J_n(p, q, r)$ is a shifted Jacobi polynomial¹ and $b_n(p, q, r)$ are weight functions guaranteeing the radial function to be orthonormal on the unit disk:

$$J_n(p, q, r) = \frac{\Gamma(n + 1)\Gamma(q)}{\Gamma(p + n)} \sum_{k=0}^n \frac{\Gamma(n + k + p)(-r)^k}{\Gamma(k + 1)\Gamma(n - k + 1)\Gamma(q + k)} \quad (4)$$

¹Indeed, given (1) and by setting $\alpha = q - 1$ and $\beta = p - q$, $J_n(p, q, r)$ can be expressed from P_n up to a multiplicative factor and a shift.

and

$$b_n(p, q, r) = \left[\frac{\Gamma(q + n)\Gamma(p + n)(p + 2n)}{\Gamma(n + 1)\Gamma^2(q)\Gamma(p - q + n + 1)} (1 - r)^{p - q} r^{q - 2} \right]^{1/2} \quad (5)$$

In this case, ZMs, PZMs, OFMMs correspond to specific values of p and q , as shown in Table I.

TABLE I: Different cases under study

Moments	p	q
ZMs	$ m + 1$	$ m + 1$
PZMs	$2 m + 2$	$2 m + 2$
OFMMs	2	2

Remark 1: Given (3), (4) and (5) and for p and q chosen as in Table I, it can be easily shown that:

$$M_{n,m}^{JFM} = (M_{n,-m}^{JFM})^* \quad (6)$$

Remark 2: Three main difficulties occur with JFMs:

- As the CVD images are defined in the Cartesian coordinate system, they must be pre-processed to fit the unit-circle. This leads to quantization error.
- The double integrations are approximated by double summations. These latter must be computed accurately to preserve as much as possible properties such as the orthogonality, the scale and rotation invariance of the moment magnitudes.
- As the moments depend on the Gamma function, directly computing high-order moments may be intensive and lead to numerical instability.

To address the three above issues, the reader may refer to [19] [20] [12] [4] [18].

2) Gegenbauer Moment family including LMs:

First of all, let us define the Gegenbauer polynomials $G_n^{(\lambda)}(x)$ of order n and scaling parameter $\lambda > -\frac{1}{2}$. Various expressions exist, based on the hypergeometric function for instance. The Gegenbauer polynomials can be also deduced from the Jacobi polynomials introduced in (1) with $\alpha = \beta = \lambda - 1/2$:

$$G_n^{(\lambda)}(x) = \frac{(2\lambda)_n}{(\lambda + \frac{1}{2})_n} P_n\left(\lambda - \frac{1}{2}, \lambda - \frac{1}{2}, x\right) \quad (7)$$

Gegenbauer polynomials are orthogonal over the square $[-1, 1] \times [-1, 1]$ with the weights $w_G(x, \lambda) = (1 - x^2)^{\lambda - \frac{1}{2}}$:

$$\int_{-1}^1 w_G(x, \lambda) G_n^{(\lambda)}(x) G_m^{(\lambda)}(x) dx = \rho_G(n, \lambda) \delta(n, m) \quad (8)$$

with $\rho_G(n, \lambda) = \frac{2\pi\Gamma(n+2\lambda)}{2^{2\lambda}n!(n+\lambda)!\Gamma(\lambda)^2}$ the normalization constant. Legendre polynomials² and Chebyshev polynomials of the 1st or 2nd kind correspond to specific values of λ , as shown in Table II.

Then, orthogonal Gegenbauer moments $M_{n,m}^G$ of order (n, m) of the CVD $f(x, y)$ are defined as follows:

$$M_{n,m}^G = \frac{1}{\rho_G(n, \lambda)\rho_G(m, \lambda)} \times \int_{-1}^1 \int_{-1}^1 f(x, y) G_n^{(\lambda)}(x) G_m^{(\lambda)}(y) w_G(x, \lambda) w_G(y, \lambda) dx dy \quad (9)$$

²Another definition is the following: $G_n^{(\frac{1}{2})}(x) = \frac{1}{2^n n!} \frac{d^n [(x^2 - 1)^n]}{dx^n}$, where $\frac{d^n [\cdot]}{dx^n}$ denotes the n^{th} derivative with respect to x and with $G_0^{(\frac{1}{2})}(x) = 1$.

Remark: As explained for JFMs, the double integration must be replaced by a double summation to take into account all the pixels of the image. This leads to approximated Gegenbauer moments. Several authors have therefore focused their attentions on this issue for the last years [7] [14].

TABLE II: *Polynomials for specific values of λ*

Polynomials	λ
Legendre polynomials	1/2
Chebyshev polynomials of the first kind	0
Chebyshev polynomials of the second kind	1

3) Discrete family - Krawtchouk moments (KMs):

KMs have been used in various applications such as face recognition [11]. The Krawtchouk polynomials of order n for N_x discrete samples $x = 0, \dots, N_x - 1$ is defined by:

$$K_n(x, \mu_x, N_x - 1) = {}_2F_1(-n, -x, -(N_x - 1), \frac{1}{\mu_x}) \quad (10)$$

where ${}_2F_1(a, b, c, z) = \sum_{k=0}^{+\infty} \frac{(a)_k (b)_k}{(c)_k} \frac{z^k}{k!}$ denotes the hypergeometric function and μ_x is in the interval $]0, 1[$. This latter plays a key role to focus on a region of interest [22].

Given the weights $w_K(x, \mu_x, N_x - 1) = \frac{(N_x - 1)!}{(N_x - 1 - x)! x!} (\mu_x)^x (1 - \mu_x)^{N_x - 1 - x}$, the Krawtchouk polynomials satisfy the orthogonality property:

$$\sum_{x=0}^{N_x - 1} w_K(x, \mu_x, N_x - 1) K_n(x, \mu_x, N_x - 1) K_m(x, \mu_x, N_x - 1) = \rho_K(n, \mu_x, N_x - 1) \delta(n, m) \quad (11)$$

where $\rho_K(n, \mu_x, N_x - 1) = (-1)^n \left(\frac{1 - \mu_x}{\mu_x}\right)^n \frac{n!}{(-N_x + 1)_n}$. The normalized version of the Krawtchouk polynomials are given by:

$$\overline{K}_n(x, \mu_x, N_x - 1) = K_n(x, \mu_x, N_x - 1) \sqrt{\frac{w_K(x, \mu_x, N_x - 1)}{\rho_K(n, \mu_x, N_x - 1)}} \quad (12)$$

At this stage, given the digital image $f(x, y)$ with $x = 0, \dots, N_x - 1$ and $y = 0, \dots, N_y - 1$, the 2-D KMs are defined as follows:

$$M_{n,m}^K = \sum_{x=0}^{N_x - 1} \sum_{y=0}^{N_y - 1} f(x, y) \overline{K}_n(x, \mu_x, N_x - 1) \overline{K}_m(y, \mu_y, N_y - 1) \quad (13)$$

They are position, scale and rotational invariant.

D. Step 4: classification

At this stage, up to a given maximum order n_{max} and a maximum repetition m_{max} , the moduli of orthogonal moments are computed and stored in a vector F . For JFMs, given (6), only positive repetition values m are considered.

After normalizing the vector F , various classification approaches can be considered including K-nearest neighbor (KNN) or support vector machine (SVM).

III. COMPARATIVE STUDY

Different variants of the above processing chain based on ZMs, PZMs, OFMMs, LMs and KMs are compared. We took advantage of recent papers [18] [3] [17] [16] [2] to accurately compute the moments, to reduce as much as possible their computational costs and to avoid numerical instabilities.

A. Simulation protocols

Let us consider a set of data defined as the sum of the returns from N_b aircraft propeller blades [10]. The k^{th} sample of the signal $s(k)$ disturbed by an additive zero-mean white noise $b(k)$ is defined, with $k = 0, \dots, N - 1$, as follows:

$$y(k) = s(k) + b(k) \quad (14)$$

$$= \sum_{l=0}^{N_b - 1} A_r L \text{sinc} \left(\frac{4\pi f_0 L}{c} \cos(\theta) \sin \left(w_r \frac{k}{f_s} + \frac{2\pi l}{N_b} \right) \right) \times e^{j \left[w_c \frac{k}{f_s} - \frac{4\pi f_0}{c} \left(R + v \frac{k}{f_s} + \frac{L_1 + L_2}{2} \cos(\theta) \sin \left(w_r \frac{k}{f_s} + \frac{2\pi l}{N_b} \right) \right) \right]} + b(k)$$

where L_1 and L_2 are respectively the distance of the blade roots and tips from the center of the rotation. Moreover, by introducing L the main blade length, $L_2 = L + L_1$. In addition, w_c and w_r are the radian frequencies of the transmitted signal and of the rotation respectively. A_r denotes the scale factor and $f_s = 10240 \text{ Hz}$ the sampling frequency. R , v , and θ are the range of the center of rotation, the radial velocity of the center of rotation with respect to the radar, and the angle between the plane of rotation and the line of sight from the radar to the center of rotation respectively. $f_0 = 5 \text{ GHz}$ and $c = 3 \times 10^8 \text{ m/s}$ denote the radar operative frequency and the speed of light respectively. Four classes have been simulated, each comprises 3000 realizations of $N = 10240$ samples with the parameters given in Table III. The rotor center location is $(0, 0, 0)$ and the radar location is $(500, 0, 500)$.

TABLE III: *Parameters defining 4 classes of signals*

Class	N_b	L (m)	L_1 (m)	L_2 (m)	w_r (rad/s)
C1	2	4	0.5	4.5	10
C2	2	6	0.5	6.5	6
C3	3	4	0.5	4.5	10
C4	3	6	0.5	6.5	6

The resulting spectrograms and CVDs of each class are given in Fig. 1, where the signal-to-noise-ratio (SNR), *i.e.* the ratio between the powers of s and b , is equal to 5 dB.

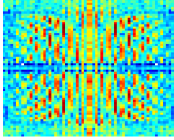
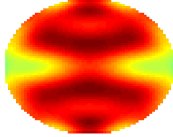
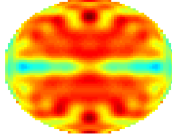
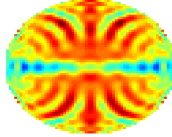
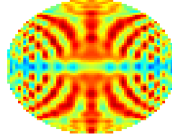
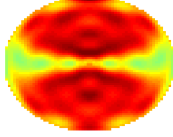
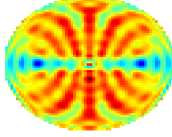
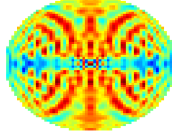
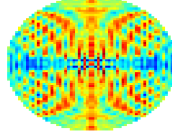
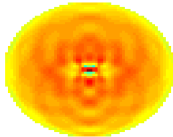
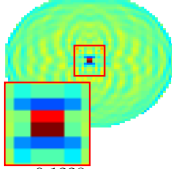
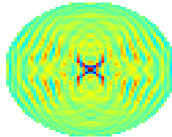
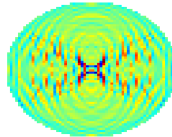
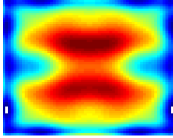
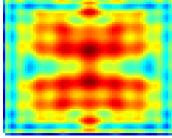
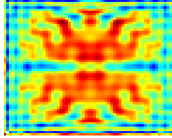
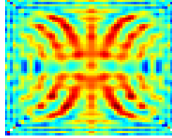
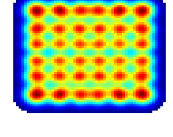
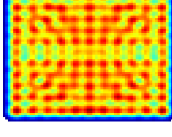
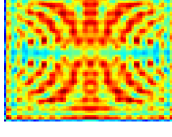
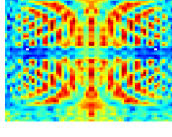
Concerning the classification step, KNN is here used with 70% of the simulated data for the training set and 30% for the test set. The rate of correct classification is averaged over 375 randomly-drawn training sets.

B. Results and comments

1) About step 3 dealing with feature extraction:

Let us analyze the decomposition of the image using various types of moments with different orders.

TABLE IV: Reconstructed CVD of the micro-Doppler (class C2) based on each family of moments versus order

Original CVD	Moments family	Order (n_{max})			
		10	20	30	40
	ZMs	 $\epsilon = 0.0790$	 $\epsilon = 0.0406$	 $\epsilon = 0.0253$	 $\epsilon = 0.0171$
	PZMs	 $\epsilon = 0.0553$	 $\epsilon = 0.0256$	 $\epsilon = 0.0137$	 $\epsilon = 0.0082$
	OFMMs	 $\epsilon = 0.1302$	 $\epsilon = 0.1228$	 $\epsilon = 0.1193$	 $\epsilon = 0.1184$
	LMs	 $\epsilon = 0.3419$	 $\epsilon = 0.7161$	 $\epsilon = 0.8757$	 $\epsilon = 0.8687$
	KMs $\mu_x = \mu_y = 0.5$	 $\epsilon = 0.4419$	 $\epsilon = 0.1110$	 $\epsilon = 0.0119$	 $\epsilon = 0.0028$

The reconstructed image, $\hat{f}(x, y)$, based on a finite number of kernels, can be obtained as follows:

$$\hat{f}(x, y) = \sum_n \sum_m M_{n,m}^{(\cdot)} \Psi_{n,m}(x, y) \quad (15)$$

In (15), the moments $M_{n,m}^{(\cdot)}$ are equal to $M_{n,m}^{JFM}$, $M_{n,m}^G$ and $M_{n,m}^K$ when the kernels $\Psi_{n,m}(x, y)$ respectively correspond to $J_{n,m}(p, q, x, y)$ with p and q defined in Table 1, $G_n^{(1/2)}(x)G_m^{(1/2)}(y)$, and $\overline{K}_n(x, \mu_x, N_x - 1)\overline{K}_m(y, \mu_y, N_y - 1)$. In this case, the normalized error made on the reconstructed image, denoted as ϵ , can be expressed as follows:

$$\epsilon = \frac{\sum_x \sum_y (f(x, y) - \hat{f}(x, y))^2}{\sum_x \sum_y (f(x, y))^2} \quad (16)$$

As described in the papers presenting the algorithms computing OFMMs and LMs, very high intensities may appear in the vicinity of the center of the unit disk of the reconstructed images when using OFMMs. With LMs, as the reconstructed images may have very high intensities at the edge of the unit disk, the corresponding pixels have been removed in the

figures given in Table IV to make the visual comparison easier. These phenomena have a strong impact on the reconstruction error. For the other methods, given Table IV, the higher the order is, the smaller ϵ is and the larger the number of details of the image can be obtained. According to the various tests we did for the different classes, the reconstruction error becomes the smallest most of the time with KMs when the order becomes higher.

Although no detail can be given about the computational cost for the lack of space, KMs provides the best compromise in terms of computational cost and accuracy.

2) *About step 4 dealing with classification:*

In Table V, the results are good even for small orders. Selecting large orders is not useful for this simulation protocol.

IV. CONCLUSIONS AND PERSPECTIVES

A comparative study of different types of moments is carried out to classify micro-Doppler features when the signal is disturbed by an additive white noise. KMs turn out to be good candidates. The simulation protocol considered serves as a first

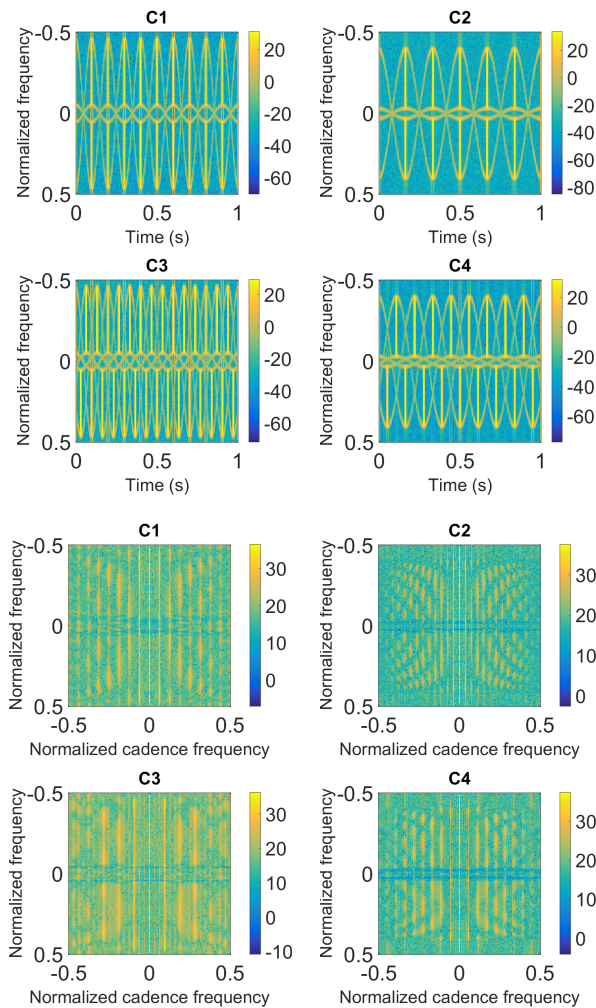


Fig. 1: Examples of spectrograms and CVDs for the 4 classes with $SNR = 5$ dB

TABLE V: Average correct-classification rate (%)

Moments family	Order							
	1	2	3	4	5	6	7	8
ZMs	84.2	99.6	99.7	100	100	100	100	100
PZMs	94.4	99.9	100	100	100	100	100	100
OFMMs	91.9	99.3	99.9	99.9	99.9	99.9	99.9	100
LMs	80.1	94.9	96.8	99.1	99.4	99.8	99.9	99.9
KMs	98.8	100	100	100	100	100	100	100

step in our study. The next step is to provide a theoretical analysis to explain why KMs are more relevant especially for small orders. Then, we will evaluate the relevance of this approach, by applying other time-frequency analysis, analyzing other moments (such as the Chebyshev, Dual Hahn and Racah ones), using other classification methods, considering time-variations of some parameters and more realistic disturbances such as some clutter and applying the method to real data.

REFERENCES

- [1] B. Bhatia and E. Wolf. On the circle polynomials of Zernike and related orthogonal sets. *Proc. Cambridge Philos. Soc.*, 50:40–48, 1954.
- [2] A. Chiang and S. Liao. Image analysis with symmetry properties of Legendre moments. *2nd International Conference on Image, Vision and Computing (ICIVC)*, pages 386–390, 2017.
- [3] C. Chonga, P. Raveendranb, and R. Mukundanc. A comparative analysis of algorithms for fast computation of Zernike moments. *Pattern Recognition*, 36, (3):731–742, 2003.
- [4] C. Clemente, L. Pallotta, A. De Maio, J. J. Soraghan, and A. Farina. A novel algorithm for radar classification based on Doppler characteristics exploiting orthogonal Pseudo-Zernike polynomials. *IEEE Trans. on Aerospace and Electronic Systems*, 51, (1):417–430, 2015.
- [5] L. Du, Y. Ma, B. Wang, and H. Liu. Noise-robust classification of ground moving targets based on time-frequency feature from micro-doppler signature. *IEEE Sensors Journal*, 14, (8):2672–2682, 2014.
- [6] S. Farokhi, U. U. Sheikh, J. Flusser, and B. Yang. Near infrared face recognition using Zernike moments and Hermite kernels. *Information Sciences*, 316:234–245, 2015.
- [7] K. M. Hosny. Image representation using accurate orthogonal Gegenbauer moments. *Pattern Recognition Letters*, 32, (6):795–804, 2011.
- [8] J. Li and H. Ling. Application of adaptive chirplet representation for isar feature extraction from targets with rotating parts. *IEE Proceedings - Radar, Sonar and Navigation*, 150, (4):284–291, 2003.
- [9] L. Liu, D. McLernon, M. Ghogho, W. Hu, and J. Huang. Ballistic missile detection via micro-doppler frequency estimation from radar return. *Digital Signal Processing*, 22, (1):87–95, 2012.
- [10] J. Martin and B. Mulgrew. Analysis of the theoretical radar return signal from aircraft propeller blades. *IEEE International Radar Conference*, pages 569–572, 1990.
- [11] S. M. Mahbubur Rahman, T. Howlader, and D. Hatzinakos. On the selection of 2D Krawtchouk moments for face recognition. *Pattern Recognition*, 54:83–93, 2016.
- [12] J. Sáez-Landete. Comments on fast computation of Jacobi-Fourier moments for invariant image recognition. *Pattern Recognition*, 67:16–22, 2017.
- [13] Y. Sheng and L. Shen. Orthogonal Fourier-Mellin moments for invariant pattern recognition. *J. Opt. Soc. Am.*, 11, (6):1748–1757, 1994.
- [14] H. Shu, L. Luo, X. Bao, W. Yu, and G. Han. An efficient method for computation of Legendre moments. *Graphical Models*, 62, (4):237–262, 2000.
- [15] C. Singh and A. Aggarwal. An efficient approach for image sequence denoising using Zernike moments-based non-local means approach. *Computers and Electrical Engineering*, 62:330–344, 2017.
- [16] C. Singh and R. Upneja. Accurate computation of orthogonal Fourier-Mellin moments. *Journal of Mathematical Imaging and Vision*, 44, (3):411–431, 2012.
- [17] C. Singh and R. Upneja. Accurate calculation of high-order pseudo-Zernike moments and their numerical stability. *Digital Signal Processing*, pages 95–106, 2014.
- [18] C. Singh, E. Walia, and R. Upneja. Accurate calculation of Zernike moments. *Information Sciences*, 233, (1):255–275, 2013.
- [19] R. Upneja. Accurate and fast Jacobi-Fourier moments for invariant image recognition. *Optik - International Journal for Light and Electron Optics*, 127, (19):7925–7940, 2016.
- [20] R. Upneja and C. Singh. Fast computation of Jacobi-Fourier moments for invariant image recognition. *Pattern Recognition*, 48, (5):1836–1843, 2015.
- [21] Y. Wang, X. Wu, W. Li, Z. Li, Y. Zhang, and J. Zhou. Analysis of micro-doppler signatures of vibration targets using EMD and SPWVD. *Neurocomputing*, 171, (1):48–56, 2016.
- [22] P. T. Yap, R. Paramesran, and S. H. Ong. Image analysis by Krawtchouk moments. *IEEE Trans. on Image Processing*, 12, (11):1367–1377, 2003.
- [23] Q. Zhang, Y. Luo, and Y. Chen. Micro-doppler characteristics of radar targets. *Elsevier, ISBN: 978-0-12-809861-5*, 2016.
- [24] R. Zhang, G. Li, and Y. D. Zhang. Micro-doppler interference removal via histogram analysis in time-frequency domain. *IEEE Trans. on Aerospace and Electronic Systems*, 52, (2):755–768, 2016.

Acknowledgment: this work was supported by GIS Albatros, the scientific cluster between Bordeaux campus and Thales. We would like also to thank C. Clemente for the exchanges we have with him about his work on PZMs.